



# Flow Control in a Cavity with Tiny-Obstacles on the Walls for Mixing Enhancement Part I: Flow Physics

B. Maneshian<sup>1,2†</sup>, K. Javadi<sup>2</sup> and M. Taeibi Rahni<sup>2</sup>

<sup>1</sup>*Aerospace Research Institute (Ministry of Science, Research and Technology), Tehran, Iran*

<sup>2</sup>*Department of Aerospace Engineering, Sharif University of Technology, Tehran, Iran*

†Corresponding Author Email: [kjavadi@sharif.edu](mailto:kjavadi@sharif.edu)

(Received October 15, 2017; accepted August 11, 2018)

## ABSTRACT

This paper seeks to make a study on flow control in two-dimensional square cavities having obstacles on their walls. The goal of using these passive controllers is to enhance mixing in an enclosed space. Lattice Boltzmann method is used to simulate the problem. Results are presented for various Reynolds numbers,  $400 \leq Re \leq 4000$  and different arrangements of tiny-obstacles with different heights. To give a perspective on the physics of this problem, time evolution of the flow is studied at  $Re = 1000$ . Then, the flow structure is studied for different Reynolds numbers. Findings show that the interaction of the main vortex with the tiny-obstacles inserted on the wall cavity changes the flow pattern at higher Reynolds numbers totally which is of high importance for mixing, such that the main primary vortex turns into a scooplike vortex along the upper wall. Also, merging the two bottom corner vortices forms a main secondary vortex which fills the cavity. Results show that obstacles heights and the gap between the upper wall and the upper obstacle are key parameters from flow control and mixing viewpoint. Also, the number of tiny-obstacles can be considered as another tool in this regard. The spaces between the obstacles don't have much influence on the flow behavior. Obstacles with  $\delta \leq 2\%$  don't change the flow field and can't be considered as a flow control tool.

**Keywords:** Flow control; Mixing enhancement; Lid-driven cavity; Tiny-obstacle; Scooplike vortex; Lattice boltzmann method.

## NOMENCLATURE

$c$	basic speed on the lattice	$v$	velocity in $y$ – direction
$e_\alpha$	discrete lattice velocities	$w_\alpha$	weight factor in the $\alpha$ direction
$f_\alpha$	distribution function	$\alpha$	direction of the link
$f_\alpha^{eq}$	equilibrium distribution function	$\delta$	percentage of the obstacle height based on the cavity length
$L$	width of square cavity	$\nu$	kinematic viscosity
$P$	pressure	$\rho$	density
$Re$	Reynolds number	$\tau$	relaxation time
$t$	time	$\Omega_\alpha$	collision operator
$U$	velocity of the cavity upper wall		
$u$	velocity in $x$ – direction		

## 1. INTRODUCTION

The lid-driven cavity flow and heat transfer within it are topics of great interest due to their frequent use in many applications. The understanding of the recirculating flow within the cavity is one of the fundamental challenges of flow control field, mixing and computational fluid dynamics (CFD) research. This problem is often experienced in many engineering and industrial applications, such as solar ponds, cooling of electronic devices, heat

exchangers, ventilation and air conditioning (HVAC) systems, materials processing, crystal growth, dynamics of lakes and metal coating and casting and therefore has been studied extensively (Chang and Chen 1999; Siegel and Nazaroff 2003; Saha *et al.* 2008; Sidik and Rahman 2009; Mustafizur *et al.* 2011). The first major researches of two-dimensional lid-driven cavity flows are done by Burggraf (1996) for the square cavity and by Pan and Acrivos (1967) for other geometrical aspect ratios. Their findings were extended by Goodrich *et al.*

1990; Shen (1991); Miller (1995) who numerically calculated the time-dependent two-dimensional cavity flows.

Many studies are directed to steady solution of the driven cavity and have presented the numerical solution of steady incompressible Navier-Stokes equations. Benjamin & Denny (1979); Ghia *et al.* (1982); Schreiber and Keller (1983); Liao & Zhu (1996); Barragy and Carey (1997); Erturk *et al.* (2005); Erturk and Gokcol (2006) have presented solutions of steady 2-D incompressible flow in a driven cavity for  $Re \leq 10000$ . Also, researches carried out by Fortin *et al.* (1997); Gervais *et al.* (1997); Sahin and Owens (2003); Abouhamza and Pierre (2003) are examples of two-dimensional hydrodynamic stability studies on driven cavity flows.

There are very few experimental studies in the literature on the driven cavity flow. Koseff & Street (1984a, 1984b, 1984c) Prasad & Koseff (1989); Znaien *et al.* (2012); Fernando *et al.* (2014) have done several experiments on three dimensional driven cavity.

In engineering applications, the geometries that exist are more complicated than a simple enclosure filled with a fluid. The geometric configuration of interest is with the presence of bodies set within the enclosure (Lacroix 1992; Ghaddar and Thiele 1994; Saha 2000). Numerous investigations applying different methods of solution on lid-driven cavity flow involving various combinations of cavity configurations and various fluids have been published in the literature. Mercan and Atalik (2009) studied high-Reynolds number lid-driven flow in arc-shape cavities with different cross sections up to  $Re = 8000$ . Yang *et al.* (2014) analyzed the flow pattern in a two-dimensional lid-driven semi-circular cavity based on multiple relaxation time lattice Boltzmann method (MRT LBM). Kalita and Gogoi (2014) carried out a global stability analysis of the flow inside a two sided staggered lid-driven cavity for both the parallel and anti-parallel motions of the lids. Vicente *et al.* (2011) studied spanwise-periodic double-sided lid-driven cavity flows with complex cross-sectional profiles. Montessori *et al.* (2014) studied the exactness and performance of the regularized version of the single-relaxation-time lattice Boltzmann equation for the case of two- and three-dimensional lid-driven cavities. The regularized version showed to provide a considerable gain in stability over the standard single-relaxation time, at a moderate computational overhead.

One of the most important applications of this problem is in heat transfer engineering. In this regard, several investigators have dealt with conjugate heat transfer inside an enclosure with the presence of a body. Nikfar and Mahmoodi (2012) investigated laminar natural convection of  $Al_2O_3$ -water nanofluid in a cavity with wavy side walls. House *et al.* (1990) numerically examined the effect of a centered, square, heat conducting body on natural convection in a vertical square enclosure. Lacroix and Joyeux (1995); Oh *et al.* (1997); Shuja *et al.* (2000); Mustafizur Rahman *et al.* (2008); Zheng *et al.* (2013); Yapicia and Obut (2015) are

those who studied mixed convection heat transfer in cavities with different conditions.

Previous researches show that although lid-driven cavities have been studied in a great deal, but most of them include physical phenomena study for different shapes and geometries. So, studying this problem from flow control and mixing augmentation viewpoint has been less notified, by now. Therefore, the main purpose of the current research is to study the problem from practical aspects and analyze the flow physics and heat transfer in cavities with details in order to find effective flow control parameters which lead to mixing augmentation. To this end, the findings are presented in two parts. In the first part which is performed in this paper, the flow physics along with different flow control parameters are studied, while the second part focuses on the effects of tiny-obstacles on mixing enhancement and heat transfer in an enclosed cavity.

In continuance, section 2 presents the problem and the governing equations. In section 3, the lattice Boltzmann method and boundary conditions are performed. In section 4, the results are validated and then, physics in time evolution and effects of Reynolds number on the flow dynamics are studied. Additionally, effects of different control parameters are explained completely.

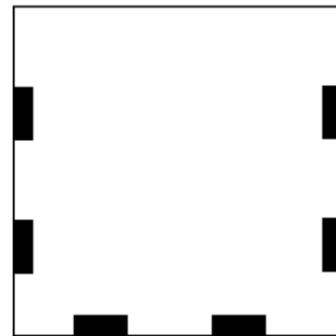


Fig. 1. A schematic configuration of a square cavity with obstacles on three walls.

## 2. PROBLEM DESCRIPTION

Fig. 1 shows a schematic configuration of a two-dimensional square cavity with obstacles on three walls which are stationary. The top wall has no obstacle and experiences a constant velocity of magnitude  $U$ . It is assumed that the fluid in the cavity is isothermal, Newtonian and incompressible with constant properties.

The equations governing the fluid flow are the Navier-Stokes equations. These equations are as follow in Cartesian-coordinates (Mendu and Das 2013):

$$\frac{\partial u}{\partial x} + \frac{\partial v}{\partial y} = 0, \quad (1)$$

$$\frac{\partial u}{\partial t} + u \frac{\partial u}{\partial x} + v \frac{\partial v}{\partial y} = -\frac{1}{\rho} \frac{\partial p}{\partial x} + \nu \left( \frac{\partial^2 u}{\partial x^2} + \frac{\partial^2 u}{\partial y^2} \right), \quad (2)$$

$$\frac{\partial v}{\partial t} + u \frac{\partial v}{\partial x} + v \frac{\partial v}{\partial y} = -\frac{1}{\rho} \frac{\partial p}{\partial y} + \nu \left( \frac{\partial^2 v}{\partial x^2} + \frac{\partial^2 v}{\partial y^2} \right), \quad (3)$$

in which,  $u$  and  $v$  are the velocities in  $x$  - and  $y$  - directions, respectively,  $\nu$  is the kinematic viscosity,  $\rho$  is the density and  $p$  is the pressure.

### 3. NUMERICAL METHOD

#### 3.1. LBM with BGK Approximation

The lattice Boltzmann method (LBM) has achieved much success in simulating hydrodynamic problems. Unlike conventional computational fluid dynamics (CFD) methods which are based on macroscopic continuum equations, the LBM solves mesoscopic kinetic equations that include the essential physics to determine macroscopic fluid flow properties. The LBM uses only local data communication to update a particle distribution function  $f_\alpha(x, t)$  at each time step. In the LBM, particle density distribution functions  $f_\alpha(x, t)$  at point  $x$  at time  $t$  are confined to move synchronously on a regular lattice, where  $\alpha$  denotes the direction of the lattice link. The distribution functions interact on the lattice in a way that conserves mass, momentum, isotropy, and Galilean invariance (Mendu and Das 2013). Here, we assume a two-dimensional and nine-velocity (D2Q9) lattice for simulation which is illustrated in Fig. 2.

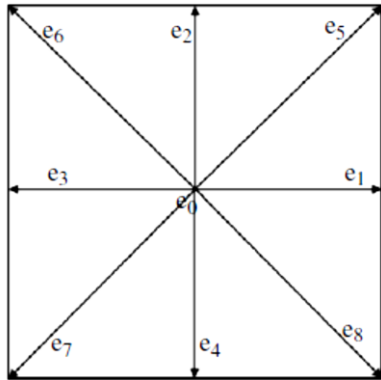


Fig. 2. Two-dimensional and nine velocity D2Q9 model.

In terms of the distribution function, the general discrete Boltzmann equation (Chen and Doolen 1998) is:

$$f_\alpha(x + e_\alpha \Delta t, t + \Delta t) = f_\alpha(x, t) + \Omega_\alpha(x, t), \quad (4)$$

where,  $e_\alpha$  represents discrete lattice velocities in the direction of link  $\alpha$ . In addition,

$$e_\alpha = (0,0) \quad \alpha = 0, \quad (5)$$

$$e_\alpha = \left[ \cos\left(\frac{\pi}{2}(\alpha - 1)\right), \sin\left(\frac{\pi}{2}(\alpha - 1)\right) \right], \quad \alpha = 1, 2, 3, 4 \quad (6)$$

$$e_\alpha = \sqrt{2} \left[ \cos\left(\frac{\pi}{2}(\alpha - 1) + \frac{\pi}{4}\right), \sin\left(\frac{\pi}{2}(\alpha - 1) + \frac{\pi}{4}\right) \right], \quad \alpha = 5, 6, 7, \quad (7)$$

where,  $f_\alpha(x, t)$  is the particle density distribution

function and  $\Omega_\alpha(x, t)$  is the collision operator (Chen and Doolen 1998; Succi 2001) as

$$\Omega_\alpha(x, t) = -\frac{1}{\tau} [f_\alpha(x, t) - f_\alpha^{eq}(x, t)], \quad (8)$$

in which,  $\tau$  is the relaxation time. The equilibrium distribution function for D2Q9 lattice model is given by

$$f_\alpha^{eq}(x, t) = w_\alpha \rho \left( 1 + 3 \frac{e_\alpha u}{c^2} + \frac{9}{2} \frac{(e_\alpha u)^2}{c^4} - \frac{3}{2} \frac{u^2}{c^2} \right), \quad (9)$$

in which,  $w_\alpha$  is the weight factor in the  $\alpha$  direction. The weight factors for the D2Q9 model are 4/9 for particles at rest ( $\alpha = 0$ ), 1/9 for particles streaming to face-connected neighbors ( $\alpha = 1, 2, 3, 4$ ), and 1/36 for particles streaming to edge-connected neighbors ( $\alpha = 5, 6, 7, 8$ );  $c$  is the basic speed on the lattice.

Macroscopic variables such as density and velocity can be obtained from the momentum integration of the particle density distribution functions as

$$\rho = \sum_{\alpha=0}^8 f_\alpha, \quad (10a)$$

$$u = \frac{1}{\rho} \sum_{\alpha=0}^8 f_\alpha e_\alpha. \quad (10b)$$

The pressure can be calculated from  $p = \rho c_s^2$  and  $c_s = 1/\sqrt{3}$ . The kinematic viscosity in relation to the relaxation factor is given by

$$\nu = \frac{2\tau - 1}{6}. \quad (11)$$

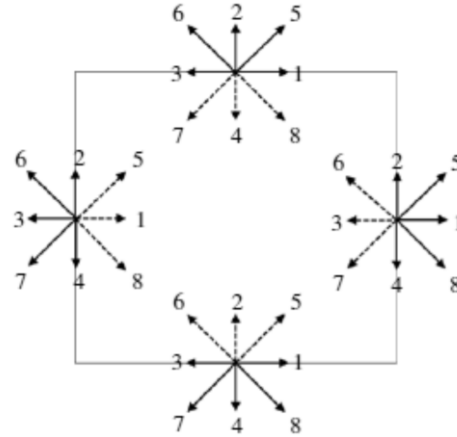
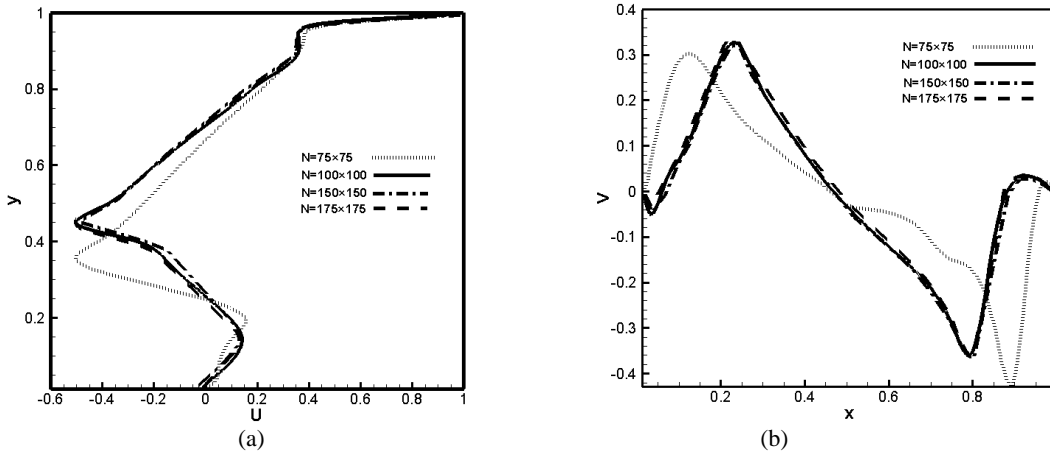


Fig. 3. Known and unknown particle density distributions for the boundaries of the cavity.

#### 3.2. Boundary Conditions

Performance of the LBM boundary conditions is simple compared to conventional CFD techniques. To perform boundary conditions, we have to calculate suitable unknown distribution functions from known distribution functions (Mendu and Das 2013). Fig. 3 illustrates the known (solid lines) and unknown (dotted lines) particle density distribution functions on all walls of the cavity. We performed the standard bounceback boundary conditions (Hou *et al.* 1995) on all fixed solid walls to calculate the unknown particle distribution functions. The particle density distribution functions on the left wall of the cavity are (Mendu and Das 2013):

$$f_1 = f_3, \quad f_5 = f_7, \quad f_8 = f_6. \quad (12)$$



**Fig. 4.** Comparison of velocity profiles for different grid sizes: a) normalized of  $u$ - velocity component along vertical line through geometric center, b) normalized of  $v$ - velocity component along horizontal line through geometric center in a cavity with two obstacles on the walls;  $Re = 4000$  and  $\delta = 3\%$ .

The particle distribution functions on the right wall of the cavity are (Mendu and Das 2013):

$$f_3 = f_1, \quad f_6 = f_8, \quad f_7 = f_5. \quad (13)$$

The particle distribution functions on the bottom wall of the cavity are (Mendu and Das 2013):

$$f_2 = f_4, \quad f_5 = f_7, \quad f_6 = f_8. \quad (14)$$

On the moving wall, the equilibrium distribution functions are used to compute the unknown particle distribution functions. The particle density distribution functions on the moving wall are (Mendu and Das 2013):

$$f_4 = \frac{1}{9}\rho \left[ 1 - 3v + \frac{9}{2}v^2 - \frac{3}{2}(u^2 + v^2) \right], \quad (15)$$

$$f_7 = \frac{1}{36}\rho \left[ 1 + 3(-u - v) + \frac{9}{2}(u + v)^2 - \frac{3}{2}(u^2 + v^2) \right], \quad (16)$$

$$f_8 = \frac{1}{36}\rho \left[ 1 + 3(u - v) + \frac{9}{2}(u - v)^2 - \frac{3}{2}(u^2 + v^2) \right]. \quad (17)$$

## 4. RESULTS AND DISCUSSIONS

In this section, findings of the present study are illustrated. First, the results are validated with the results related to standard cavity reported by other researchers. In continuance, physics of flow in time evolution is studied. In the later sections, effects of Reynolds number, obstacles heights, numbers of obstacles, the space between upper wall and the upper obstacle and the space between obstacles are investigated.

### 4.1. Verification and Validation of LBM Code

Grid resolution study was performed to check grid independency of the results. In this regard, the cavity with two obstacles on the walls and  $\delta = 3\%$  ( $\delta$  is the percentage of the obstacles height based on the cavity length) was chosen. To show grid independency of the results, the centerline  $u$  - and  $v$  - velocity

profiles were examined over four different grid sizes of  $75 \times 75$ ,  $100 \times 100$ ,  $150 \times 150$  and  $175 \times 175$  as illustrated in Fig. 4. The cavity Reynolds number  $Re = \frac{UL}{\nu} = 4000$ , where  $L$  is the width of the square cavity,  $U$  is the velocity of upper wall and  $\nu$  is the kinematic viscosity. Comparison of the profiles demonstrates that the grid size of  $100 \times 100$  is appropriate to simulate the flow structure.

In addition, observation is directed toward lid-driven flows in square cavities. Simulations are first applied for a standard cavity with different Reynolds numbers. In order to examine the results, the centerline  $u$  - and  $v$  - velocity profiles for two different values of Reynolds number are compared with the results by Ghia *et al.* (1982) in Fig. 5a and Fig. 5b. Comparison between present results and those reported by Ghia *et al.* (1982) shows excellent consistency which demonstrates the precision of the results. In addition, Fig. 5c and Fig. 5d illustrate flow patterns in standard cavities in two mentioned different Reynolds numbers.

### 4. 2. Physics of the Flow in Time Evolution

To give a perspective of flow pattern, **Error! Reference source not found.** illustrates time evolution of flow behavior in a cavity when it has two obstacles on each wall with the  $\delta = 5\%$  ( $\delta$  is the percentage of the obstacles height based on the cavity length). As it can be seen, in the first seconds, the movement of the upper wall affects the fluid in its neighbor and creates a small vortex there. By increasing the time,  $t = 0.3s$ , a separation bubble is appeared between two obstacles in the right hand side. The core of this separation bubble is near the upper obstacle. At time  $t = 0.4s$ , this bubble has grown toward the lower part of the obstacle and at  $t = 0.5s$ , this bubble grows and is drawn to the left hand side which creates a rotational zone that contains all the back area of the main vortex. The separated area grows by time and has tendency to merge with the right corner vortex of the bottom and then gradually, moves to the center of the cavity. At  $t = 0.6s$ , this merged vortex unites with the left corner vortex and contains all the lower part of the

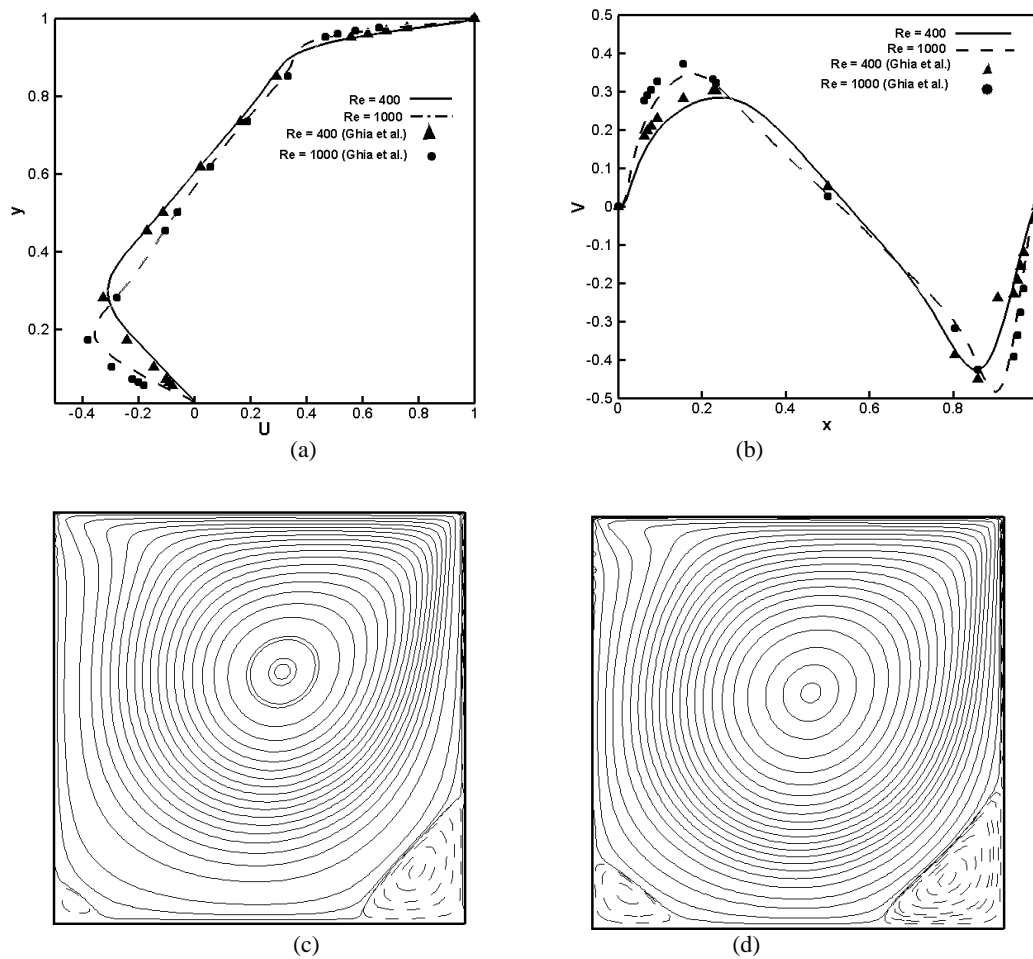


**Fig. 5. Comparison of velocity profiles of a standard cavity with the results reported by Ghia *et al.* (1982) for various Reynolds numbers: a) normalized of u- velocity component along vertical line through geometric center, b) normalized of  $v_x$  velocity component along horizontal line through geometric center, c) flow pattern in standard cavity for  $Re = 400$ , d) flow pattern in standard cavity;  $Re = 1000$ .**

cavity. As can be seen clearly, there is a saddle point at left where these two vortices meet each other. At  $t = 0.7s$ , the saddle point has disappeared. By increasing time, the new created vortex has grown more and its core will move to the left hand side, gradually. At  $t = 1.2s$ , a vortex appears in the right corner of the bottom. By passing time, two vortices are organized in the corners of the bottom which can be seen at  $t = 1.5s$ . The secondary vortex will grow more by time and its core will move toward the upper wall. Finally, at  $t = 20s$ , this process will cause to have two vortices in the cavity, one scooplike vortex in the upper part of the cavity which is driven by the lid surface and another in the lower part in a counter direction driven by the upper vortex. The scooplike vortex which is in the space between the upper wall and upper obstacle has high frequency and exchanges its momentum to the secondary vortex. During this process, the position of the center of the upper vortex is fixed up to  $t = 4s$ , approximately.

#### 4. 3. Effect of Reynolds Number

To have a better understanding of the flow field, effects of Reynolds number on flow pattern are

investigated. For this purpose, the cavities with the same arrangement and having two obstacles on each wall are considered. Fig. 6 shows that when  $Re = 400$ , two corner vortices of the bottom have merged into a unit vortex and it has a saddle point in the left hand side. This new vortex has two cores; one in the right hand and the other in the left hand side of the cavity. When Reynolds number increases to 600, this created vortex has grown in size, has one core in the right hand and its saddle point is disappeared. Also, a small vortex can be seen in the right bottom corner. Increasing Reynolds number more, causes the secondary vortex to grow more and its core moves to the left. Finally, in  $Re = 1000$ , the primary vortex is moved to the top right and lay in the space between the upper wall and the upper obstacle. This vortex has high frequency and exchanges its momentum to the secondary vortex which rotates in a counter direction. For  $Re \geq 900$ , two vortices can be seen in the bottom corners, too.

#### 4. 4. Effect of Obstacles

This section underlines the effects of obstacles on the flow pattern in cavities having obstacles on their

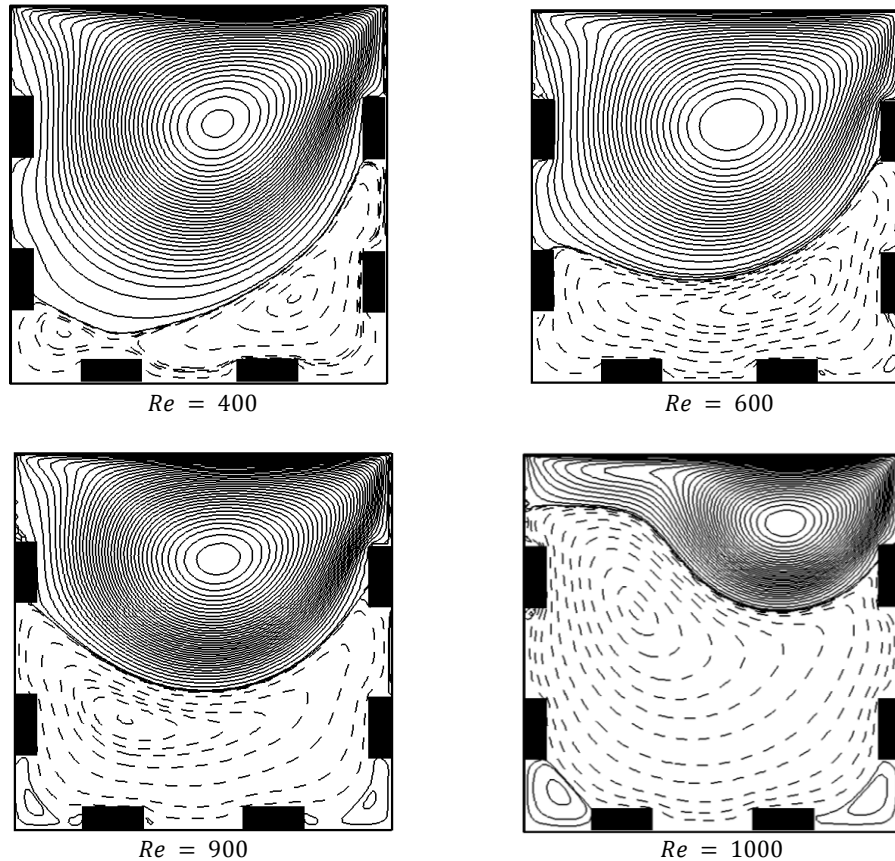


**Fig. 6.** Effects of Reynolds number on the flow field in cavities with two obstacles on each wall with  $\delta = 5\%$ .

walls. So, in part (a), cavities with  $\delta = 2\%$  and different numbers of obstacles are considered. Part (b) regards obstacles with  $\delta \geq 3\%$  and various arrangements.

**Part a) Obstacles with  $\delta = 2\%$**

Streamline patterns of the flow in cavities with one and two obstacles on each wall are illustrated in Fig. 7a to Fig. 7f. In these cases, flow pattern is similar to the standard cavity (having no obstacles). It is implied from these figures that by increasing the Reynolds number, a small vortex would appear on the top left corner and two corner vortices of the bottom grow, as was expected (Fig. 7c and Fig. 7f). Consequently, obstacles with  $\delta = 2\%$  don't have considerable effect on the flow pattern in comparison with the standard cavity. In other words, the flow can't sense the obstacles in the cavity. Therefore, the obstacles with  $\delta \leq 2\%$  can't be considered as a flow control tool in such cavities and cannot alter the heat transfer coefficients or mixing characteristics effectively. For this reason, the cavities having obstacles with  $\delta \geq 3\%$  are investigated.

**Part b) Obstacles with  $\delta \geq 3\%$**

In this part, effects of different parameters such as obstacle heights, obstacle numbers and the space between the obstacles are studied. To investigate the effects of the obstacles height on the flow pattern, two cases of cavities,  $\delta = 3\%$  and  $\delta = 5\%$ , are considered.

Flow patterns in cavities with one obstacle arranged, irregularly on each wall are illustrated in Fig. 8. As demonstrated in this figure, for  $\delta = 3\%$ , the global flow pattern is like standard cavity. However, enlargement of the obstacles height controls the flow pattern, such that when  $Re = 400$ , the two corner vortices of the bottom merge into a secondary vortex and a saddle point forms in the left hand side (compare Fig. 8a and Fig. 8d). As the Reynolds number increases further by enlarging the height of the obstacles, the left vortex of the merged vortices grows in size and the saddle point moves toward up right hand side. Finally, for  $\delta = 5\%$  when Reynolds number increases from 1000 to 4000, the structure of the flow pattern will change drastically as illustrated in Fig. 8f. In this case, the saddle point disappears and a main secondary vortex is created which fills the whole cavity. In addition, two vortices appear in bottom corners and the main primary vortex moves to the top right hand side and forms a scooplike one. Another important point that should be considered is that two bottom corner vortices in Fig. 8f are mirror in shape and opposite direction with two bottom corner vortices in Fig. 8c. As a consequence, enlargement of the obstacles height has a great effect on the control of the flow in such cavities and can be considered as a key parameters in heat transfer and mixing problems.

To continue, effects of obstacles numbers on the flow control in the cavity is investigated. In this regard,

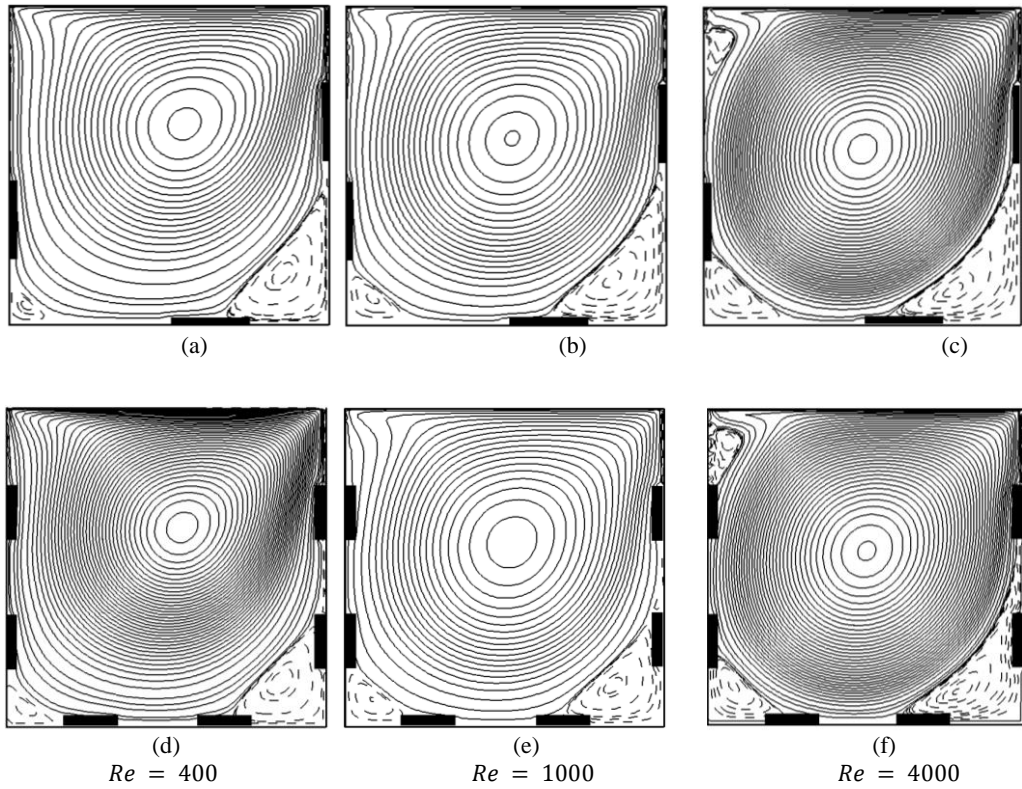


**Fig. 7.** Flow patterns for condition of one (top) and two obstacles (bottom) on each wall of a square cavity with  $\delta = 2\%$ .

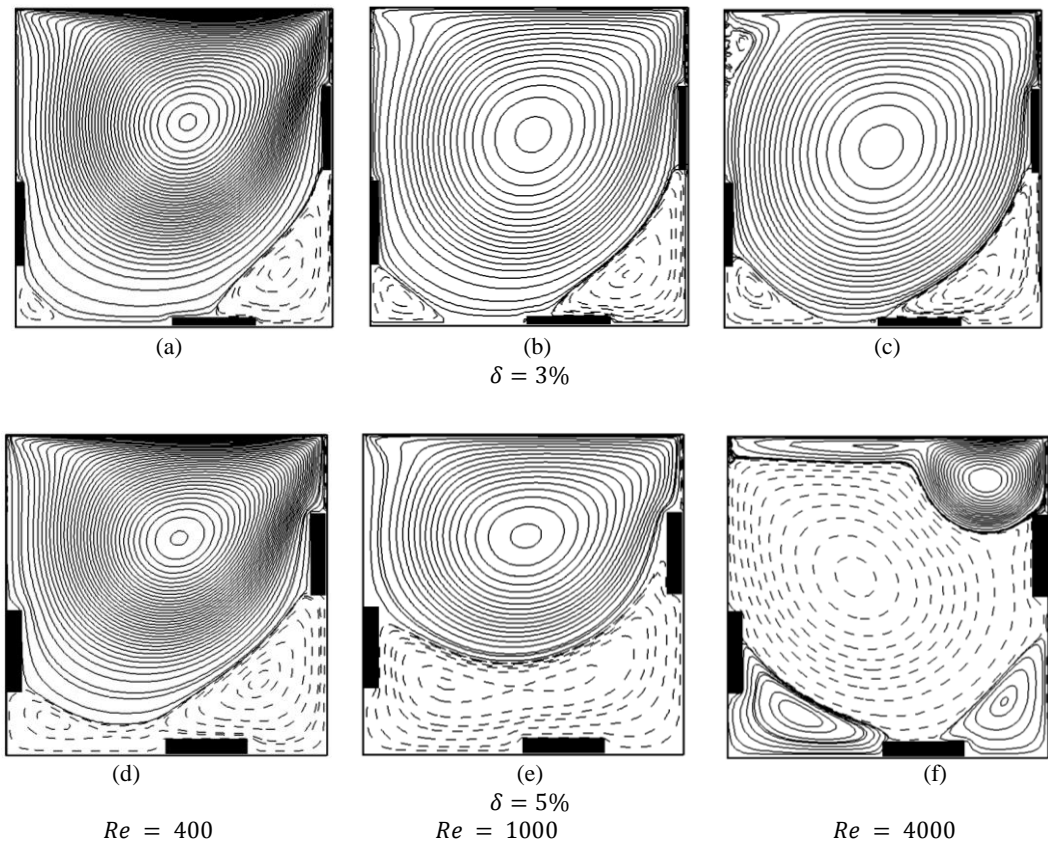


**Fig. 8.** Flow patterns for condition of irregular arrangement of three obstacles in a square cavity with  $\delta = 3\%$  and  $\delta = 5\%$ .

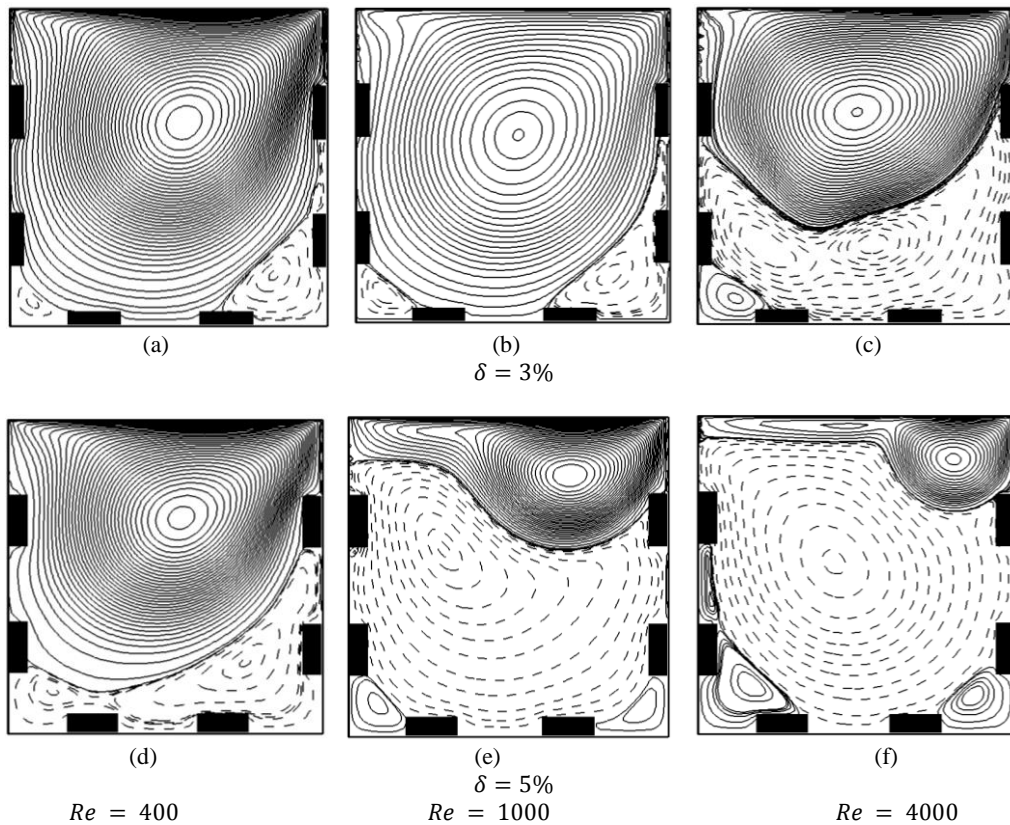


**Fig. 9.** Flow patterns for condition of two obstacles on each wall of a square cavity with  $\delta = 3\%$  and  $\delta = 5\%$ .

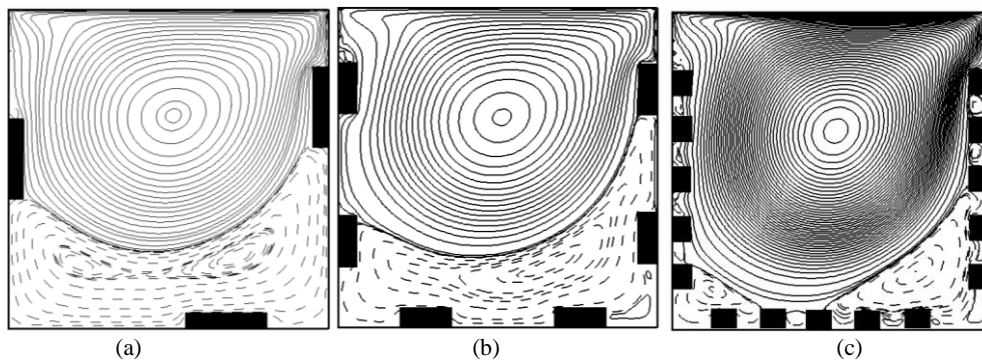


**Fig. 10.** Flow patterns for condition of cavities with obstacles with  $\delta = 5\%$  and  $Re = 1000$ , a) one obstacle b) two obstacles and c) three obstacles on each wall.

flow patterns in cavities with one, two and five obstacles on each wall are considered which will be discussed as follow.

Fig. 9 presents the flow pattern in cavities with two obstacles on each wall. Comparison of Fig. 8 and Fig. 9 shows that in  $Re = 400$ , there is no difference between the flow patterns for  $\delta = 3\%$  and  $5\%$ . However for higher Reynolds numbers this is not the case. As can be seen from Fig. 8 and Fig. 9, for  $\delta = 3\%$  the flow structure for  $Re = 1000$  are the same (compare Fig. 8b and Fig. 9b). While for  $Re = 4000$ , the flow pattern is completely different (compare Fig. 8c and Fig. 9c). This is vice versa for  $\delta = 5\%$  (compare Fig. 8e and Fig. 9e, Fig. 8f and Fig. 9f).

The flow pattern in Fig. 9c exhibits that two corner vortices of the bottom have merged into a unit vortex with a saddle point near center and two cores in both sides. Also, a vortex is observed in the bottom left hand side.

To study the effects of numbers of obstacles on the flow pattern in such cavities, three different cases are investigated in Fig. 10. In case (a) there is one obstacle on each wall. The two corner vortices of the bottom are merged into a unit vortex with two cores in the right and left hand sides and a saddle point near the center. In case (b) the space between the upper wall and the upper obstacle is equal to the corresponding space in case (a) but the number of obstacles is increased to two. In this case, the corner

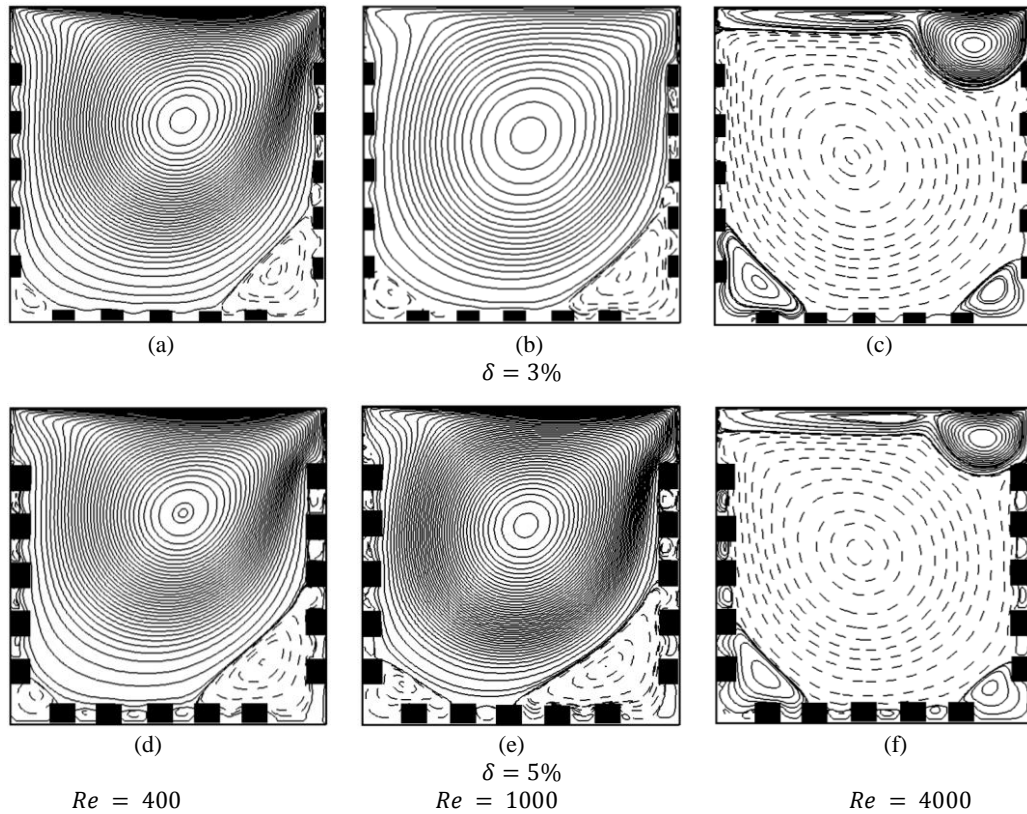


**Fig. 11.** Flow patterns for condition of five obstacles on each wall of a square cavity with  $\delta = 3\%$  and  $\delta = 5\%$ .

vortices of the bottom are merged completely with a core in the right hand side and no saddle point. Also, a vortex is formed in the right bottom of the cavity. In case (c), number of obstacles equals to five and the space between the upper wall and the upper obstacle is equal to the corresponding space in previous cases (a) and (b). Flow pattern in this case is the same as the flow pattern in standard cavities. Additionally, the flow is trapped between the obstacles and behaves like a micro closed cavity. In Fig. 11, number of obstacles is increased to five on each wall. Visualization of the flow pattern in Fig. 11 shows that cases a, b, d and e are like standard cavities. But flow structures in Fig. 11c and f change. In these two cases, the primary main vortex appears in the area between the upper wall and the upper obstacle, scooplike vortex, the main secondary vortex is formed and two corner vortices are appeared in the bottom. On the other hand, comparison of Fig. 11e and Fig. 9e shows that for  $Re = 1000$  and  $\delta = 5\%$ , increasing the number of obstacles leads to changes in the flow pattern due to the increase of the obstacles numbers and decrease of the distance between the upper wall and the upper obstacle (Fig. 11e). Another finding in Fig. 11 is that in  $Re = 4000$ , enlargement of the obstacle height causes the scooplike vortex to be smaller and grow less in comparison to the case with  $\delta = 3\%$ .

Consequently, as illustrated in Fig. 10 and Fig. 11, increasing the number of obstacles alone without considering other parameters doesn't have always positive effects on mixing augmentation or heat

transfer improvement in all flow regimes.

The space between the obstacles is another point which should be investigated. Fig. 12 studies the flow pattern in three cases. In case (b) in comparison to case (a), the upper obstacle is in its previous position and the lower obstacle is moved downward. So, the space between obstacles is increased. The global flow patterns in these two cases are the same. The difference is that in case (b), the secondary vortex has grown more in size and a corner vortex is created in the left bottom.

In case (c) in comparison to case (a), the upper obstacle is moved downward and the lower obstacle is in its previous position. So, the space between obstacles is decreased. Flow structure in case (c) is changed drastically. The reason of these changes is not the decrease of the space between obstacles. The main reason is the increase of the space between the upper wall and the upper obstacle.

Findings show that the space between the obstacles can't be an effective parameter in controlling the flow in cavities.

#### 4. 5. Effects of the Space between upper Wall and the upper Obstacle

As mentioned before, an important point about the flow pattern in such cavities is the distance between the upper wall and the upper obstacle. In Fig. 13a, there is no space in the mentioned area. So, the flow pattern is like the case of a standard square cavity

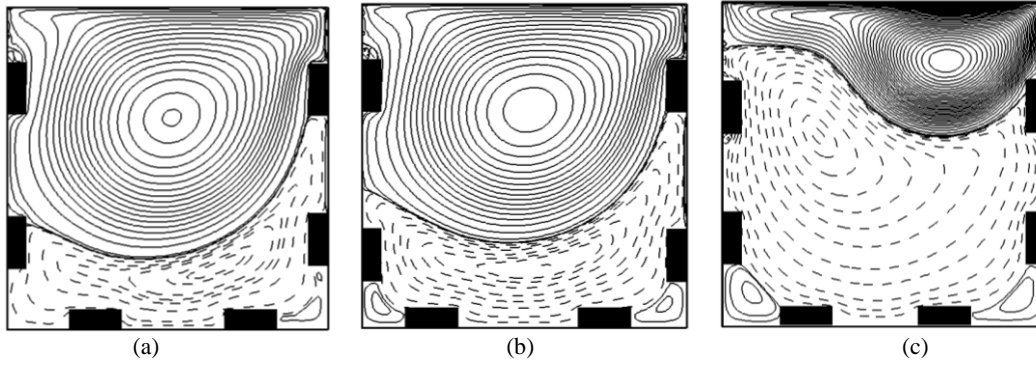


**Fig. 12.** Flow patterns for condition of two obstacles on each wall of a square cavity with two different distances between the obstacles,  $\delta = 5\%$  and  $Re = 1000$ .

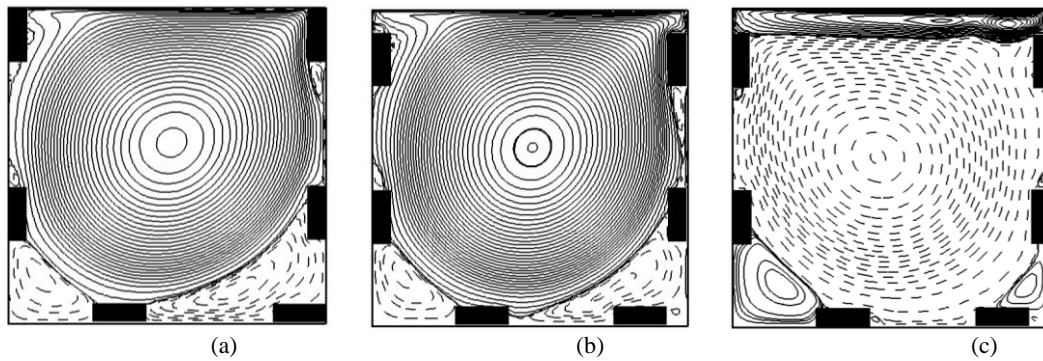


**Fig. 13.** Flow patterns in a square cavity a) when there is no space between the upper obstacle and the upper wall, b) the space between the upper obstacle and the upper wall is 8% and c) the space between the upper obstacle and the upper wall is 9% of the cavity length,  $Re = 4000$  and  $\delta = 5\%$ .

with no obstacles. In this case, the obstacle on the lower wall prevents two corner vortices of the bottom from merging and forming a saddle point in this area. Also, it is seen that two open cavities are formed in the space between two obstacles at right and left walls. Fig. 13b and Fig. 13c compare two different cases. In case b, the distance between the upper obstacle and the upper wall is 8% of the cavity length and in case c, this distance is 9%. It can be seen that flow in case (b) behaves like the flow in case (a) but, in case (c), the primary vortex is stretched, turned into a slender vortex laying in a thin layer along the moving upper wall and the secondary vortex fills the whole cavity. In addition, two bottom corner vortices in Fig. 13c are mirror in shape and opposite direction with two corresponding vortices in cases (a) and (b).

As a result, flow field is so sensitive to the space between the upper wall and the upper obstacle. This gap plays a major role on the flow control in cavities and can be considered as a key parameter for this problem.

## 5. CONCLUSIONS

This paper gives a detailed study on the flow physics in two-dimensional lid-driven cavities with the presence of obstacles on the walls in order to

make a parametric study from the flow control viewpoint. Lattice Boltzmann method (BGK approximation) is applied to simulate the problem. In this regard, results are presented for various Reynolds numbers,  $400 \leq Re \leq 4000$ , different arrangements of obstacles, different obstacle heights, different obstacles numbers, different spaces between obstacles and different gap sizes between the upper obstacle and the moving wall which are summarized as:

Time evolution of the fluid flow for the cavities with  $\delta = 5\%$  at  $Re = 1000$  shows that at first seconds, a small vortex is generated at top right corner due to the momentum exchanges between the moving wall and the neighbor fluid. With increasing time, the momentum of the upper layers diffuses to the lower layers and after a while, the whole cavity fluid turns to move in a closed path. By passing time, due to the interaction of the moving fluid with inserted obstacles on the walls, the created separation bubble at the right hand side is merged with the secondary bottom corner vortices and the big secondary vortex is formed filling all most the entire cavity. Finally, the process reaches a steady state situation which includes one scooplike vortex in the upper part, a main secondary vortex rotating in a counter direction respect to the scooplike vortex and two bottom corner vortices.

Obstacles with  $\delta \leq 2\%$  don't influence the flow field and are not recommended to be used as the flow control tools. However, further increasing of  $\delta$  creates considerable changes in the flow pattern, particularly at high Reynolds numbers. Therefore, for a fixed Reynolds number, this is an effective parameter in controlling the flow in cavities.

Numbers of obstacles along with the Reynolds number effects are other parameters that should be regarded as a tool for the control of the flow field. For a fixed Reynolds number, combined effects of obstacles numbers and the spaces between them are the factors that specify whether the two bottom corner vortices merge and grow up or not.

The distance between the upper wall and the upper obstacle has a great effect on flow pattern. If there is no distance between the upper wall and the upper obstacle, the flow pattern in the cavity is like a standard cavity. While, increasing this distance enough, causes significant changes in the flow field. This gap is determinant to have a main clock-wise rotating vortex (such as standard cavity), either to have a clock-wise rotating scoop-like vortex in the top zone of the cavity and a main secondary counter clockwise vortex below it, or to have a clock-wise rotating stretched slender vortex laying along the moving wall and a main secondary counter clockwise vortex below it. Accordingly, this factor is highly recommended to be used as a flow control mean in such cavities.

The spaces between the obstacles don't change flow features significantly. Hence, it is of minor importance from flow control point of view.

Briefly, results demonstrate that interaction of the flow with wall obstacles creates a scooplke vortex along the upper wall. The obstacles heights and the gap between the upper wall and the upper obstacle are two factors that play a major role from flow control aspect in the cavity. Obstacles numbers is another parameter that should be regarded as a tool for flow control field. On the other hand, the influence of the space between the obstacles isn't as much effective as previous parameters. Also, obstacles with  $\delta \leq 2\%$  can't influence the flow field in the cavity.

## REFERENCES

- Abouhamza, A. and R. Pierre (2003). A neutral stability curve for incompressible flows in a rectangular driven cavity. *Mathematical and Computer Modeling* 38, 141-157.
- Barragy, E. and G. F. Carey (1997). Stream function-vorticity driven cavity solutions using p finite elements. *Computers and Fluids* 26, 453-468.
- Benjamin, A. S. and V. E. Denny (1979). On the convergence of numerical solutions for 2-D flows in a cavity at large Re. *Journal of Computational Physics* 33, 340-358.
- Burggraf, O. R. (1996). Analytical and numerical studies of the structure of steady separated flows. *J. Fluid Mech* 24, 113-151.
- Chang, M. H. and C. H. Cheng (1999). Prediction of lid-driven flow and heat convection in an arc-shaped cavity. *Int. Comm. Heat Mass Transfer* 26, 829-838.
- Chen, S. and G. D. Doolen (1998). Lattice Boltzmann method for fluid flows. *Annual Rev. Fluid Mech* 30, 329-364.
- Erturk, E. and C. Gokcol (2006). Fourth order compact formulation of Navier-Stokes equations and driven cavity flow at high Reynolds numbers. *International Journal for Numerical Methods in Fluids* 50, 421-436.
- Erturk, E., T. C. Corke and C. Gokcol (2005). Numerical solutions of 2-D steady incompressible driven cavity flow at high Reynolds numbers. *International Journal for Numerical Methods in Fluid* 48, 747-774.
- Fernando, J. N., J. Kriegseis, and D. E. Rival (2014). Modal analysis of confined square and rectangular cavity flows. *International Journal of Heat and Fluid Flow* 47, 123-134.
- Fortin, A., M. Jardak, J. J. Gervais and R. Pierre (1997). Localization of hopf bifurcations in fluid flow problems. *International Journal for Numerical Methods in Fluids* 24, 1185-1210.
- Gervais, J. J., D. Lemelin and R. Pierre (1997). Some experiments with stability analysis of discrete incompressible flows in the lid-driven cavity. *International Journal for Numerical Methods in Fluids* 24, 477-492.
- Ghaddar, N. K. and F. Thiele (1994). Natural convection over a rotating cylindrical heat source in a rectangular enclosure. *Numerical Heat Transfer* 26, 701-717.
- Ghia, U., K. N. Ghia and C. T. Shin (1982). High-Re solutions for incompressible flow using the Navier-Stokes equations and a multigrid method. *Journal of Computational Physics* 48, 387-411.
- Goodrich, J. W., K. Gustafson and K. Halasi (1990). Hopf bifurcation in the driven cavity. *Journal of Computational Physics* 90, 219-261.
- Hou, S., Q. Zou, S. Chen, G. Doolen and A. C. Cogley (1995). Simulation of cavity flow by the lattice Boltzmann method. *Journal of Computational Physics* 118, 329-347.
- House, J. M., C. Beckermann and T. F. Smith (1990). Effect of a centered conducting body on natural convection heat transfer in an enclosure. *Numer. Heat Transfer* 18, 213-225.
- Kalita, J. C. and B. B. Gogoi (2014). Global two-dimensional stability of the staggered cavity flow with an HOC approach. *Computers and Mathematics with Applications* 67, 569-590.
- Koseff, J. R. and R. L. Street (1984). On end wall effects in a lid driven cavity flow. ASME

- Journal of Fluids Engineering* 106, 385-389.
- Koseff, J. R. and R. L. Street (1984). The lid-driven cavity flow: a synthesis of qualitative and quantitative observations. *ASME Journal of Fluids Engineering* 106, 390-398.
- Koseff, J. R. and R. L. Street (1984). Visualization studies of a shear driven three-dimensional recirculating flow. *ASME Journal of Fluids Engineering* 106, 21-29.
- Lacroix, M. (1992). Natural convection heat transfer around two heated horizontal cylinders inside a rectangular cavity cooled from above. *Numerical Heat Transfer* 21, 37-54.
- Lacroix, M. and A. Joyeux (1995). Natural convection heat transfer around heated cylinders inside a cavity with conducting walls. *Numer. Heat Transfer* 27, 335-349.
- Liao, S. J. and J. M. Zhu (1996). A short note on higher-order stream function-vorticity formulation of 2-D steady state Navier-Stokes equations. *International Journal for Numerical Methods in Fluids* 22, 1-9.
- Mendu, S. S. and P. K. Das (2013). Fluid flow in a cavity driven by an oscillation lid-a simulation by lattice Boltzmann method. *European Journal of Mechanics B/Fluids* 39, 59-70.
- Mercan, H. and K. Atalik (2009). Vortex formation in lid-driven arc-shape cavity flows at high Reynolds numbers. *European Journal of Mechanics B/Fluids* 28, 61-71.
- Miller, W. (1995). Flow in the driven cavity calculated by the lattice Boltzmann method. *Physical Review* 51, 3659-3671.
- Montessori, A., G. Falcucci, P. Prestininzi, M. La Rocca and S. Succi (2014). Regularized lattice Bhatnagar-Gross-Krook model for two- and three-dimensional cavity flow simulations. *Physical Review* 89, 0533171-0533178.
- Mustafizur Rahman, Md., M. A. Alim, S. Saha and M. K. Chowdhury (2008). A numerical study of mixed convection in a square cavity with a heat conducting square cylinder at different locations. *Journal of Mechanical Engineering* 39, 78-85.
- Mustafizur Rahman, Md., Md. Elias and Md. A. Alim (2011). Mixed convection flow in a rectangular ventilated cavity with a heat conducting solid square cylinder at the center. *IJE Transactions B: Applications* 4, 93-105.
- Nikfar, M. and M. Mahmoodi (2012). Meshless local Petrov-Galerkin analysis of free convection of nanofluid in a cavity with wavy side walls. *Engineering Analysis with Boundary Elements* 36, 433-445.
- Oh, J. Y., M. Y. Ha and K. C. Kim (1997). Numerical study of heat transfer and flow of natural convection in an enclosure with a heat generating conducting body. *Numer. Heat Transfer* 31, 289-304.
- Pan, F. and A. Acrivos (1967). Steady Flows in Rectangular Cavities. *J. Fluid Mech.* 28, 643-655.
- Prasad, A. K. and J. R. Koseff (1989). Reynolds number and end-wall effects on a lid-driven cavity flow. *Physics of Fluids* 1, 208-218.
- Saha, A. K. (2000). Unsteady free convection in a vertical channel with a built-in heated square cylinder. *Numerical Heat Transfer* 38, 795-818.
- Saha, S., G. Saha and Md.Q. Islam (2008). Natural convection in square enclosure with adiabatic cylinder at center and discrete bottom heating. *DIU Journal of Science and Technology* 3, 29-36.
- Sahin, M. and R. G. Owens (2003). A novel fully-implicit finite volume method applied to the lid-driven cavity flow problem part II linear stability analysis. *International Journal for Numerical Methods in Fluids* 42, 79-88.
- Schreiber, R. and H. B. Keller (1983). Driven cavity flows by efficient numerical techniques. *Journal of Computational Physics* 49, 310-333.
- Shen, J. (1991). Hopf bifurcation of the unsteady regularized driven cavity flow. *Journal of Computational Physics* 95, 228-245.
- Shuja, S. Z., B. S. Yilbas and M.O. Iqbal (2000). Mixed convection in a square cavity due to heat generating rectangular body. *Int. J. Numer. Methods Heat Fluid Flow* 10, 824-841.
- Sidik, N. A. C. and M. R. A. Rahman (2009). Mesoscale investigation of natural convection heat transfer from a heated cylinder inside square enclosure. *European Journal of Scientific Research* 38, 45-56.
- Siegel, J. A. and W. W. Nazaroff (2003). Predicting particle deposition on HVAC heat exchangers. *Atmospheric Environment* 37, 5587- 5596.
- Succi, S. (2001). *The Lattice Boltzmann Equation for Fluid Dynamics and Beyond*. Oxford University Press, Oxford.
- Vicente, J. D., D. Rodríguez, V. Theofilis and E. Valero (2011). Stability analysis in spanwise-periodic double-sided lid-driven cavity flows with complex cross-sectional profiles. *Computers and Fluids* 43, 143-153.
- Yang, F., X. Shi, X. Guo and Q. Sai (2014). MRT lattice Boltzmann schemes for high Reynolds number flow in two-dimensional lid-driven semi-circular cavity. *Computers and Mathematics with Applications* 67, 569-590.
- Yapicia, K. and S. Obut (2015). Laminar mixed-convection heat transfer in a lid-driven cavity with modified heated wall. *Heat Transfer Engineering* 36, 303-314.
- Zheng, G. F., M. Y. Ha and H. S. Yoon (2013). A numerical study on mixed convection in a lid-

B. Maneshian *et al.* / *JAFM*, Vol. 12, No.1, pp. 11-23, 2019.

driven cavity with a circular cylinder *Journal of Mechanical Science and Technology* 27, 273-286.

Znaïen, J., M. F. M. Speetjens, R. R. Trieling and H.

J. H. Clercx (2012). Observability of periodic lines in three-dimensional lid-driven cylindrical cavity flows. *Physical Review* 85, 0663201-06632014.